ARCHIVES
of
FOUNDRY ENGINEERING

ISSN (2299-2944)
Volume 2025
Issue 3/2025

168 – 178

19/3

10.24425/afe.2025.155366

Published quarterly as the organ of the Foundry Commission of the Polish Academy of Sciences

Melt Quality Assessment in Casting of A6082 Alloy

B. Tunca [a, b, *], **D. Dışpınar** [c], **L.C. Kumruoğlu** [b]

[a] R&D Department, Sistem Alüminyum San. ve Tic. A.Ş., Turkey
[b] Department of Metallurgy and Materials Engineering, Faculty of Engineering, Iskenderun Technical University, Turkey
[c] R&D Department, Foseco, Netherlands
* Corresponding author: E-mail address: bilgehantnca@gmail.com

Received 16.10.2024; accepted in revised form 12.03.2025; available online 26.08.2025

Abstract

In this study, it was aimed to examine the metallurgical structures of AA6082 alloys after the casting and homogenization process by means of changing degassing and flux ratios during melt treatment. During the casting of AA6082 alloys, billets were produced, porosity was determined by the reduced pressure test where density index (DI%), hydrogen level (ml/100 g Al) and bifilm index (BI) were examined. After the product was cast, two different homogenization process were carried out and grain sizes, microstructures and homogeneity were examined. In addition, SEM and EDS examinations were carried out and AlFeSi and Mg_2Si precipitate formations were analyzed in terms of size, number and distribution. It was found that the melt cleanliness plays a significant role on the product quality. The melt quality was increased by optimization of the nitrogen gas flow rate with a refining flux application where the elimination of the splashing of the melt surface was found to be the critical parameter. Overall, it was found that the grain size had become finer, and the homogeneity rate was increased.

Keywords: Solidification, Metallography, 6082 Alloy, Bifilm, Density Index

1. Introduction

Aluminum alloys that are to be extruded or rolled are most commonly cast by direct-chill (DC) casting. 6XXX Al alloys are used extensively in the extruded form, due to their strength, ductility, and resistance to corrosion. With its maximum strength and tolerable extrudability, the 6082 alloy in particular is becoming more and more popular in the automotive applications. Many defects that may be generated during melting and casting process can dramatically affect the final product quality. Particularly in the case of extrusions, the presence of defects will lead to cracking and premature facture resulting in decreased yield. The defects can be classified into two categories: extrinsic and intrinsic. Intrinsic defects are mainly caused by shrinkage or segregation. Mainly, undesirable Fe-based intermetallic phases can be formed which can cause hot cracking or surface defects during extrusion. The type, size, morphology, and distribution of the intermetallic particles are very important in determining the subsequent material properties. Therefore, homogenization heat treatment procedure is carried out at high temperature and holding times to eliminate the negative effects of intermetallic phases [1–5].

The transition metals such as Fe and Mn are always present. These elements have the tendency to form intermetallic phases in the presence of Si [6–10]. During the casting of 6xxx aluminum alloys a wide variety of Fe-containing intermetallics such as Al–Fe, Al–Fe–Si and Al–Fe–Mn–Si phases are formed between the aluminum dendrites [11–13]. Carlberg et al [14] reported depending on the Fe:Si ratio with regard to high segregation of Fe, α- or β phases form. As-cast billets require a homogenization treatment to make the material suitable for hot extrusion. During

this homogenization treatment several processes take place such as the transformation of interconnected plate-like β-Al_5FeSi intermetallic into more rounded discrete α-$Al_{12}(FeMn)_3Si$ particles when Mn content is around 0.5 wt.% [7] and the dissolution of β-Mg_2Si particles [11]. Many models have developed and validated to aid the heat treatment cycles to estimate the desired phase distribution and achieve the needed mechanical properties [15,16].

Extrinsic defects are mainly caused by oxides. During melting of aluminum, because of its high affinity to oxygen, an aluminum oxide layer is formed on the surface. When this surface oxide becomes entrained into the melt, the melt quality starts to decrease. The density of liquid aluminum and the entrained oxides are almost similar, therefore, these defects cannot float or sink to the bottom of the furnace. A proper refining flux is needed to remove these oxides from the melt in an aim to achieve defect-free melt with high quality castings [17-20]. Kvithyld et al [21] has extensive works on the recycling of aluminum scraps. Bocskal et al [22] reported that good quality castings of 6063 and 6082 can be achieved from 100% scrap with a proper cleaning of the melt. Rajagukguk et al [23] reported the increase of large plate-like β-Fe phases after recycling. The application of several new methods has been investigated to clean the melt prior to DC casting such as ultrasonic applications and intensive melt shearing methods [8,24,25,26].

The aim was targeted to investigate the effect of degassing and flux application on the homogeneity of the microstructure of billets as well as their final product quality.

2. Material and Methods

2.1. Billet Casting Process

The products called billets 8-inch diameter produced in this study are produced by the Direct Chill Casting method (DC casting). In this process, the liquid metal is directly solidified with water and solidified vertically.

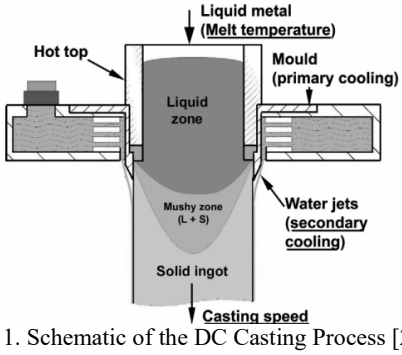

Fig. 1. Schematic of the DC Casting Process [27]

Further cooling of the ingot bulk to a temperature below the alloy solidus is achieved by quenching (cooling, chilling) the solid shell directly with water jets (Fig. 1) as the ingot descends beneath the lower edge of the mold (secondary cooling), which provides up to 95% heat extraction [27]. In D.C. casting, the as-cast structure is shaped by three factors: edge solidification from heat extraction via the mould wall, direct cooling for full solidification, and metal feed for the desired flow pattern. "Indirect cooling" through the mould wall forms a shell zone and surface segregations, major edge defects, with their extent depending on the mould wall length [28].

The chemical composition of 6082 aluminum alloy billet production is given Table 1.

Table 1.
Chemical analysis of 6082 (wt.%)

Cast	Si	Fe	Cu	Mn	Mg	Cr	Zn
1	0.82	0.20	0.06	0.49	0.65	0.08	0.01
2	0.86	0.22	0.05	0.46	0.68	0.06	0.01

2.2. Liquid Metal Quality Measurement

First, raw materials are charged into melting furnaces and melted. After the melting and alloying processes are completed, the liquid metal cleaning is carried out. Fluxes in the form of powder is introduced to the melt with nitrogen gas by flux feeder. Afterwards, the inclusions that rise to the surface are collected and only nitrogen gas is purged for few minutes without the flux. This process ensures temperature homogeneity of the liquid metal and also removes the hydrogen gas. Then the casting begins, and during the casting process, a sample is taken from the liquid metal and placed in the Reduced Pressure Test device to solidify under vacuum. A metric that can be used to quantify the melt quality based on RPT results was introduced by Dispinar and Campbell [29-32] to monitor both inclusions and hydrogen level together after digital image analysis of the cross section of the RPT sample. They proposed to measure the maximum length of pores as an indication of bifilm length and introduced a new metric, called the bifilm index (BI) [31,34]:

$$\text{Bifilm index} = \Sigma(\text{maximum length of pores}) \quad (1)$$

The bifilm index is measured by image analysis method. An RPT samples cross-section is grinded down to 600 grinding paper by metallographic methods. Then, at least 600 dpi scanning resolution is used to convert the samples cross-section into an image format (either JPG or TIFF is acceptable). Any image analysis software can be used to measure the maximum length of pores. In this study, OpenSource ImageJ software was used. After importing the image into the software, the calibration has to be made to define the dimension. Then, a threshold is applied to select all the pores. Image analysis software can measure the maximum length of selected objects, also known as the “major axis length” or “ferret length”. Then, the recorded measurements are exported into excel sheet and the sum of these data is calculated as Bifilm Index in mm.

2.3. Heat Treatment Process

The heat treatment of the AA6082 is generally carried out at sub-eutectic temperature of 580°C with a certain time to form of

the precipitate phase in the aluminum matrix. However, AA6082 alloys may have different recipes depending on the chemical composition. Therefore, temperature and time parameters may vary.

After the heat treatment process, samples are collected and subjected to microstructural analysis. For this purpose, samples are first grinded, then polished and electrochemically etched. After images are collected by optical microscope under polarized filter, the grain boundaries and grains become visible with different colorations (due to different orientation of the crystal structure). Then, image analysis tool is used to measure the grain size by ASTM E112 in which line method was used calculate the grain size. At least five lines are drawn parallel to each other with the known length. Then the intercepts of the grain boundaries are recorded which is divided by the full length of the lines thereby giving the average grain size of each sample.

The same images are also subjected to further image analysis. Very similar to bifilm index measurements. A threshold is applied to select each phase. Then, the size and distribution of these secondary phases are measured in which normal distribution curves are plotted. Then, the average size and number of these phases are compared with each other to reveal the homogeneity of the microstructures. A very fine and evenly distributed secondary phases would result in 100% homogeneity.

3. Results and Discussion

3.1. Liquid Metal Quality Measurement

In this work, the samples were taken after the liquid metal was prepared and density indices and hydrogen percentages from the RPT device are given in Table 2.

Table 2.
Cast 1 density indices and hydrogen level

Sample Name	Density Index (ID%)	Hydrogen (ml/100 g Al)
Cast 1-A: before degassing	10.6	0.352
Cast 1-B: after degassing	7.8	0.251
Cast 1-C: start of casting	7.6	0.244
Cast 1-D: during casting	7.65	0.246

The cross-sections of these samples after their density indexes and hydrogen levels were examined are shown in Figure 2.

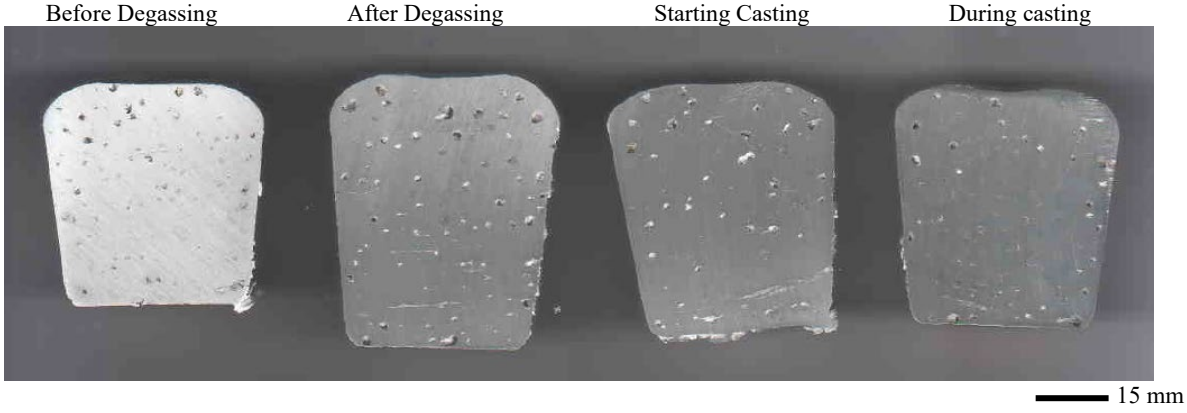

Fig. 2. Sample sections taken from the RPT device of Cast 1 and Bifilm Index

The RPT samples taken from Cast 1 were cut in half and their surfaces were prepared and then scanned for bifilm index measurements [33]. The bifilm index was examined from these samples which is shown in Figure 3.

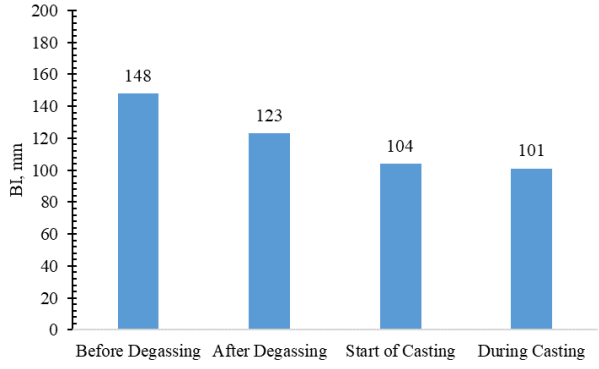

Fig. 3. Bifilm index of Cast 1

When the bifilm index is examined, there is a decrease in the bifilm index, which is an indication that the melt cleanliness gets better. However, considering that Dispinar [31] had bifilm index below 50 mm is an indication of high quality melt, based on the findings in Figure 3, it is apparent that the melt quality was not at its best for the trials in Cast 1. As can be seen from the samples taken from Cast 1, the bifilm index values are very high (Figure 3). The liquid metal cleaning process has been improved to reduce the density and bifilm index here. While doing this, studies were carried out on two basic processes. In Cast 1 trials, 25 kg of flux was added to 30 tons of liquid metal in 4 minutes, and its ratio to the total amount was around 0.08%. During the degassing process, nitrogen gas was purged into the liquid metal for approximately 20 minutes at 4 bars. While this process was being carried out, the liquid metal was splashing vigorously, and the surface was disturbed significantly. In other words, instead of cleaning, more oxides were introduced into the melt; hence the high bifilm index values.

In the next casting process (Cast 2), improvements were considered based on the observations of the previous trials. The flux application was increased to 10 minutes (from 4 minutes), 75 kg was added which is around 0.25% (compared to 25 kg in the previous trial). During the degassing process, nitrogen pressure was reduced to 2 bar and applied for a maximum of 15 minutes. The density indexes and the hydrogen level are given in Table 3.

Table 3.
Cast 2 density indices and hydrogen level

Sample Name	Density Index (DI%)	Hydrogen (ml/100 g Al)
Cast 2-A: before degassing	8.9	0.290
Cast 2-B: after degassing	6.1	0.193
Cast 2-C: start of casting	5.2	0.163
Cast 2-D: during casting	4.58	0.142

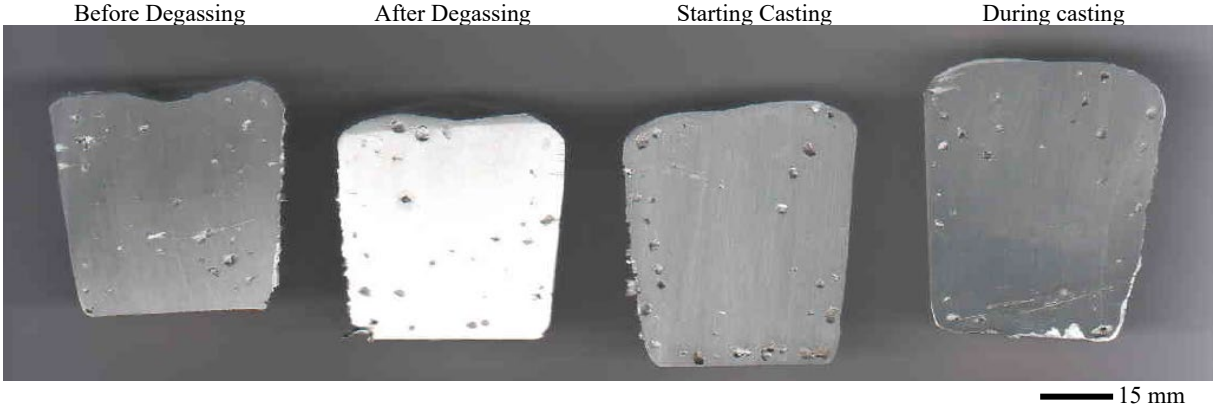

Fig. 4. Sample sections taken from the RPT device of Cast 2

RPT samples taken from Casting 2 were cut in half and their surfaces were prepared for analysis and are shown in Figure 4. The bifilm index of these samples was examined and shown in Figure 5.

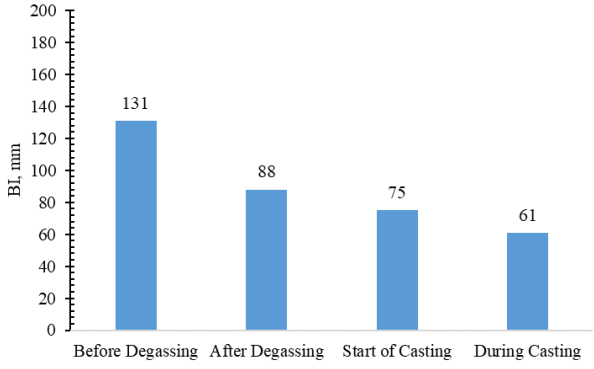

Fig. 5. Bifilm index of Cast 2

When the bifilm index of Cast 2 is examined, there is a good amount of improvement compared to Cast 1. Hydrogen levels decreased in direct proportion to the bifilm index. As a result, the degassing and cleaning were considered to be successful.

3.2. Microstructure Analysis

After the casting process, the billets were subjected to homogenization annealing, and samples are cut for microstructural analysis. After grinding and polishing, a 2% HF etching solution was used for etching. Microstructure images were viewed from the NIKON ECLIPSE MA200 instrument. The microstructures taken from the billets, which are the final products of Cast 1 and Cast 2, are shown in Figure 6 and Figure 7, respectively.

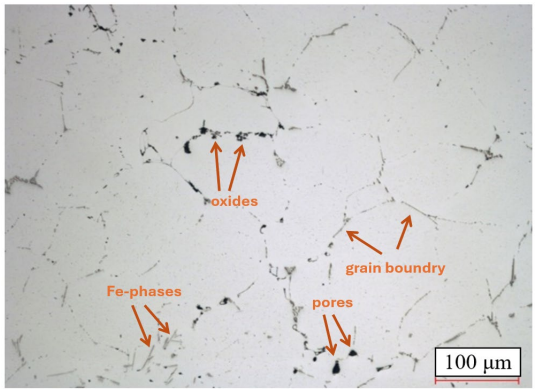

a)

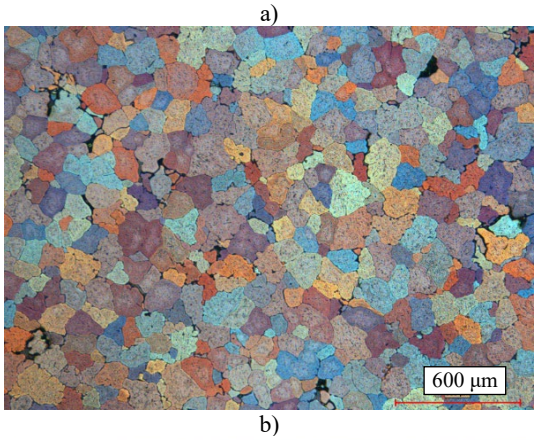

b)

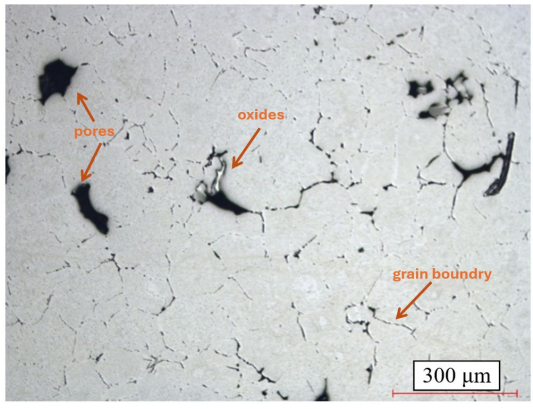

c)

Fig. 6. Cast 1 Microstructure: a) no etching, b) Barker Etching, c) 2% HF etching

The microstructure examination of Cast 1 is shown in Figure 6. A lot of defects have been detected. Coarse particulate precipitations are present. The average grain size was 159 µm. The homogeneity rate was found to be 72%.

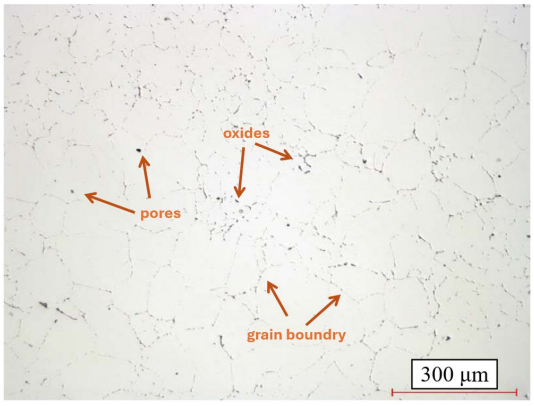

a)

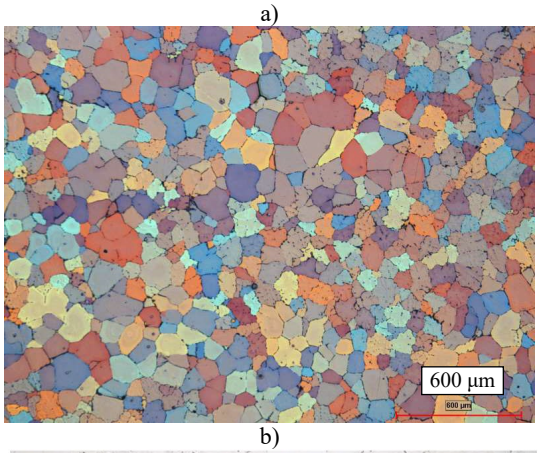

b)

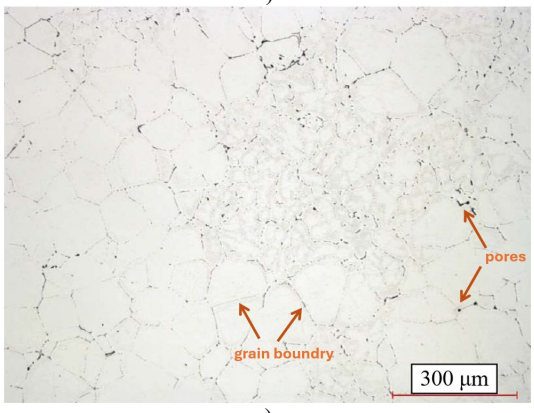

c)

Fig. 7. Cast 2 Microstructure: a) no etching, b) Barker Etching, c) 2% HF etching

The microstructure examination of Cast 2 is shown in Figure 7. The inclusion content is much lower than Cast 1. Coarse particulate precipitates are present at grain boundaries. The average grain size was 117 µm. The homogeneity rate was 80%.

Significant improvement was observed as a result of change in the degassing and fluxing application during melt treatment stage. The homogenization annealing recipe also has a great impact on these transformations. As can be seen in the SEM-EDS images in the next section, the 8-hour process at 580 °C in the first casting is excessive in terms of both time and temperature. It

was seen in the results that inclusions decreased, and grain sizes were more homogeneous at 565 °C and 7 hours process time outputs. The homogenization recipes made are given in Figure 8.

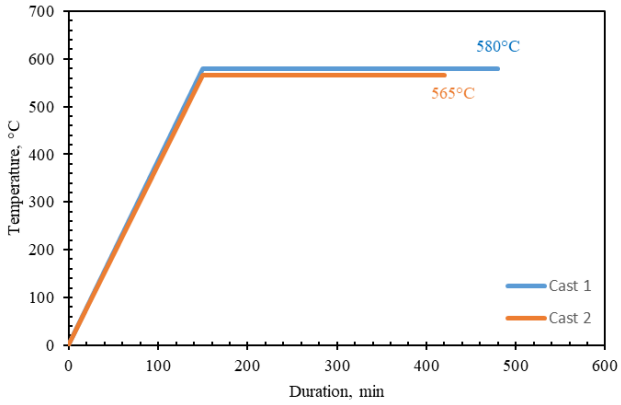

Fig. 8. Homogenization process chart of Cast 1 and 2

3.3. SEM-EDS Analysis

SEM-EDS examinations of Cast 1 and Cast 2 castings were carried out. As it is well-known, Mn and Cr elements regulate the microstructure in 6082 alloys together with Mg and Si. Without changing the morphological structure of the AlFeSi precipitates that will form as a result of this addition, this structure changes to AlFeSi(Mn,Cr) in terms of stoichiometry. There is no change in the MgSi precipitate, which is another important phase that determines the mechanical properties. Bayat [1,2] reported that Mg_2Si particles would precipitate at β-Fe particles, however, they would be dissolved during heat treatment and α-Fe nucleation would be preferred sites.

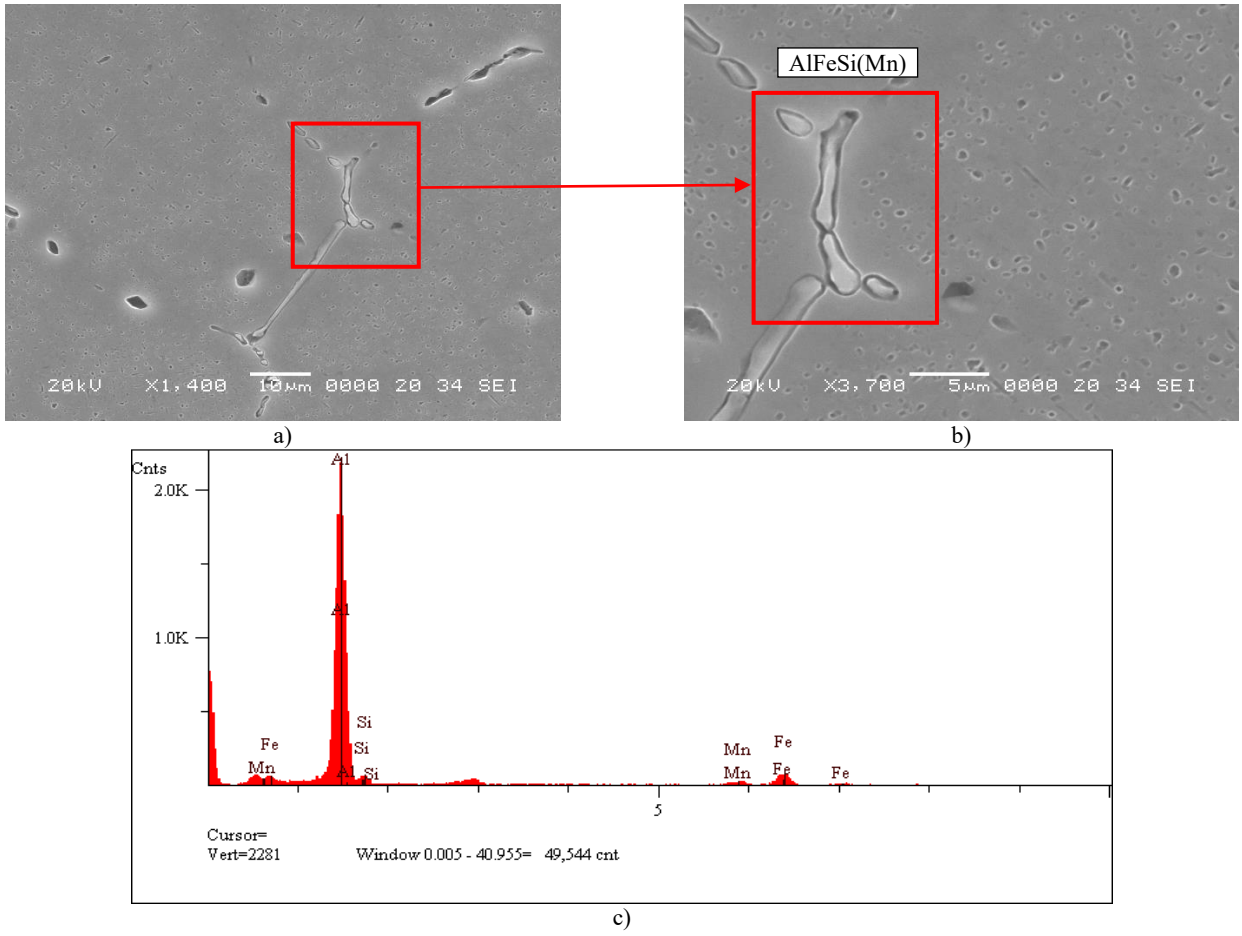

Fig. 9. Cast 1 SEM-EDS_1: a) examined microstructure, b) magnification of the area with an AlFeSi(Mn) phase, c) EDS spectrum of the AlFeSi(Mn) phase

In the SEM examinations made in Figure 9 a-b, AlFeSi(Mn) precipitate was clearly detected, as seen in the EDS analysis in Figure 9 c. In the examinations made in the central region of Cast 1, coarse particles were detected in the grain structure. This is mainly due to inhomogeneous heat treatment. In addition, it is known that the oxides present in the microstructure have the tendency to nucleate Fe-based intermetallic phases. The presence of these precipitates may cause an increase in surface tearing and/or unexpected decreases in final mechanical properties, especially during extrusion. Engler et al [3] had shown the harmful effects and have these can be removed by homogenization treatments. For this reason, the formation of such precipitates should be prevented in which melt cleanliness plays a significant role such that removal of oxides would hinder the nucleation of Fe-phases.

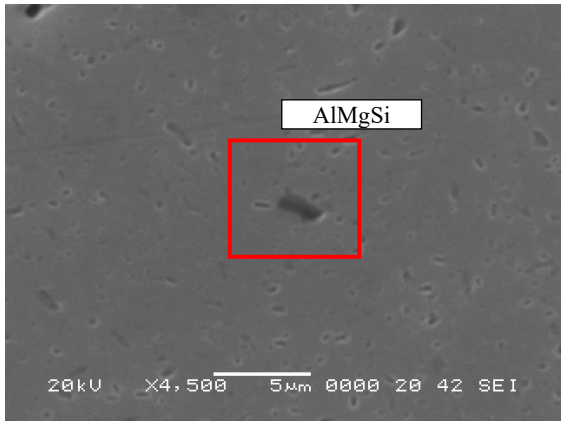

a)

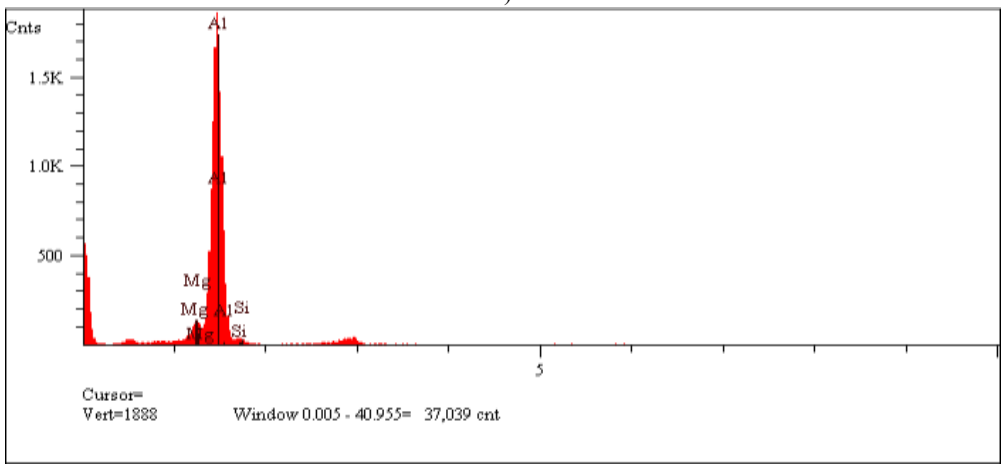

b)

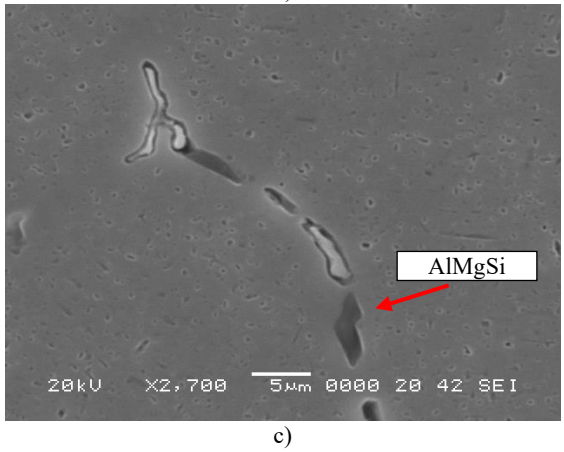

c)

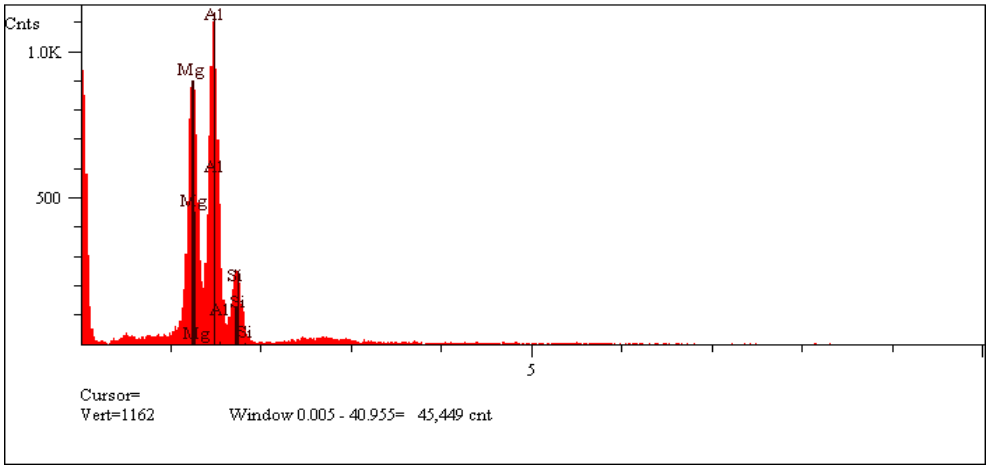

d)

Fig. 10. Cast 1 SEM-EDS_2: a) precipitation of the AlMgSi phase, b) EDS spectrum of the AlMgSi phase, c) precipitation of the AlMgSi phases, d) EDS spectrum of the AlMgSi phase

A typical microstructure of AA6082 material is given in Figure 10. A grain boundary precipitates are observed in this structure. Two different precipitates have been identified. It is AlMgSi-based precipitate that appears as dark gray (Figure 10 d). This type of structure is again an undesirable formation [3]. What is desired is for the MgSi precipitates is to be able to finely distributed within the grain as much as possible [9]. It should not be forgotten that MgSi precipitates, which have a eutectic structure, may accelerate hot tearing during extrusion if they precipitate at the grain boundary (especially in a coarse form). Another point that should be taken into consideration is that although the billet casting and subsequent homogenization processes are completed perfectly, a similar structure may occur when the billet remains in the heating furnace for a long time for any reason during the billet preheating processes [11,12]. SEM images of Cast 2 are given in Figure 11 below.

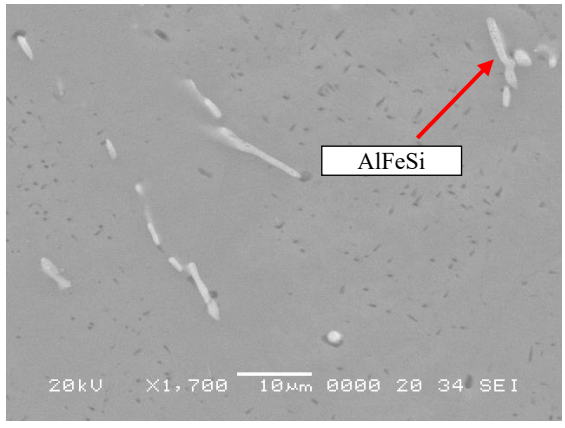

a)

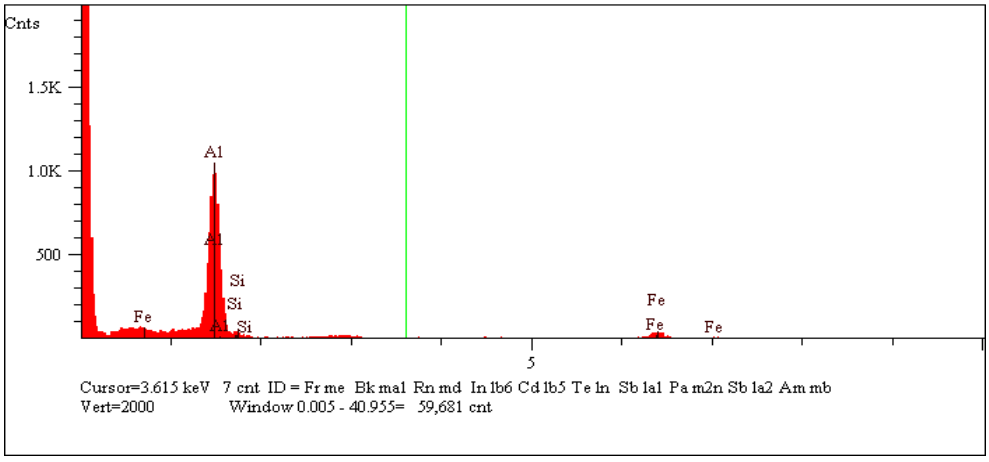

b)

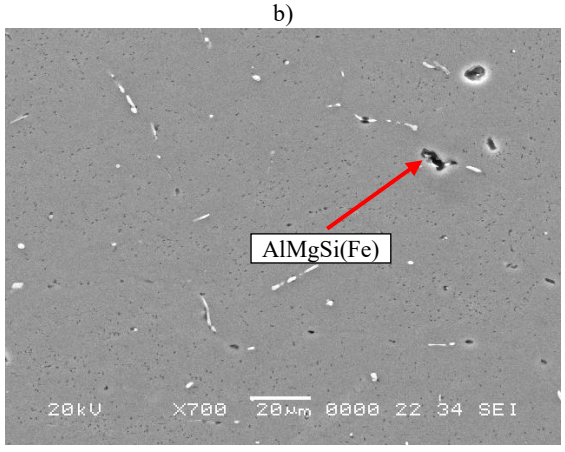

c)

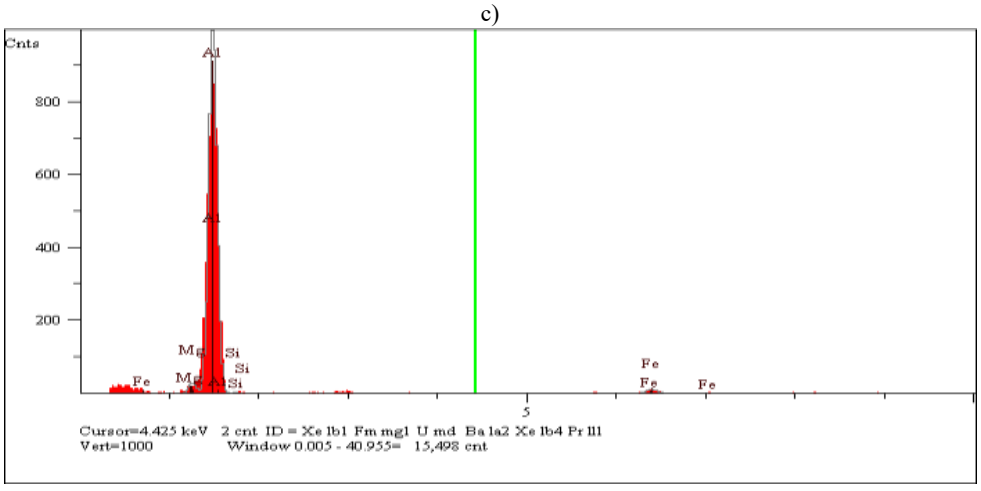

d)

Fig. 11. Cast 2 SEM-EDS: a) area with an AlFeSi phase, b) EDS spectrum of the AlFeSi phase, c) area with an AlMgSi(Fe) phase, d) EDS spectrum of the AlMgSi(Fe) phase

SEM scanning and EDS analysis were performed on two different regions: inside the grain and at the grain boundary. Precipitates are found to be in the edge of the billet. However, as going towards the center of the billet, coarser sediment structures are encountered. In Figure 11(a), coarse AlFeSi particles are observed in the places indicated by arrows. In Figure 11(b), the EDS analysis in this region is examined. Micro voids were found in Figure 11(c). EDS analysis of AlMgSi(Fe) is given in Figure 11(d). It has been understood that they generally form in the grain boundary region. This is also where oxides are carried in which

the nucleation of Fe-phases becomes easier. Similarly, AlFeSi peaks were detected in EDS analysis made from grain boundaries. Sarafoglu et al [16] showed that α-Fe phase formation was enhanced when Si dissolution was increased during homogenization. Kumar [8] suggested that α-Al grain structure had no effect on the phase selection of α- or β-Fe phase formations. Khan et al [7] reported that 0.5 wt.% Mn would lead to α-$Al_{15}(Fe,Mn)_3Si_2$ being the major intermetallic phase solidifying in the 1.0 wt.% Fe containing alloy.

When the SEM-EDS analysis of two different castings was examined, there were precipitates at the grain boundaries and coarse particles were formed. Despite this, there are still improvements in Cast 2 compared to Cast 1.

4. Conclusions

In this study, the difficulties experienced in the casting and annealing process of AA6082 alloy were discussed. In these castings, the defects that are formed due to improper degassing and flux application as well as the heterogeneity of the microstructures based on melt quality were assessed. A general evaluation of the study is summarized as follows:

1. By increasing the amount of flux used in the liquid metal cleaning stage from 0.08% to 0.25%, the cleaning (removal of oxides and impurities) has been increased.
2. The nitrogen gas used during the degassing process was reduced from 4 bar to 2 bar and the degassing time was shortened by 5 minutes. In this way, oxides formed due to splashing (which generated more bifilms), were removed from the liquid metal.
3. The density indexes of the samples taken during casting were reduced from 7.65 to 4.58% and the hydrogen level decreased from 0.246 to 0.142 ml/100 g Al.
4. The bifilm index was 101 mm during improper cleaning process which was reduced to 61 mm and a 40% improvement was achieved by controlled degassing and flux application.
5. The homogenization parameter was changed from 580 to 565°C, and the duration was shortened by 1 hour and which resulted in the improvements of the microstructure.
6. When billet microstructures were examined, the grain size was decreased from 159 μm to 117 μm. The amount of homogeneity increased from 71 to 80%. With improved melt cleanliness.
7. SEM images revealed a decrease in the formation of coarse particles after the changes in the process as indicated above.

References

[1] Bayat, N. & Carlberg, T. (2017). Influence of heat treatment on the surface structure of 6082 Al alloys. *Metallurgical and Materials Transactions A*. 48, 5085-5094. https://doi.org/10.1007/s11661-017-4207-6.

[2] Bayat, N., Carlberg, T. & Cieslar, M. (2017). In-situ study of phase transformations during homogenization of 6005 and 6082 Al alloys. *Journal of Alloys and Compounds*. 725, 504-509. https://doi.org/10.1016/j.jallcom.2017.07.149.

[3] Engler, O., Schröter, T. & Krause, C. (2023). Formation of intermetallic particles during solidification and homogenisation of two Al–Mg–Si alloys. *Materials Science and Technology*. 39, 70-84. https://doi.org/10.1080/02670836.2022.2102279.

[4] Tunca, B., İnce, B. & Deniz, D. (2025). Enhancing liquid metal quality in aluminum alloys: a study on refining techniques. *Journal of Engineering Research and Reports.* 27(2), 104-113. https://doi.org/10.9734/jerr/2025/v27i21398.

[5] Izcankurtaran, D., Tunca, B. & Karatay, G. (2021). Investigation of the effect of grain refinement on the mechanical properties of 6082 aluminium alloy. *Open Journal of Applied Sciences*. 11(6), 699-706. https://doi.org/10.4236/ojapps.2021.116051.

[6] Warmuzek, M., Gazda, A., Sieniawski, J. & Mrówka, G. (2003). Processes of the formation of the Fe (Mn)-bearing intermetallic phases in the Al-Fe-(Mn)-Si alloys. *Advances in Materials Science*. 3(2), 81-91.

[7] Khan, M.H., Das, A., Li, Z. & Kotadia, H.R. (2021). Effects of Fe, Mn, chemical grain refinement and cooling rate on the evolution of Fe intermetallics in a model 6082 Al-alloy. *Intermetallics*. 132, 107132, 1-10. https://doi.org/10.1016/j.intermet.2021.107132.

[8] Kumar, S. & O'Reilly, K. (2016). Influence of Al grain structure on Fe bearing intermetallics during DC casting of an Al-Mg-Si alloy. *Materials Characterization*. 120, 311-322. https://doi.org/10.1016/j.matchar.2016.09.017.

[9] Liu, C., Azizi-Alizamini, H., Parson, N., Poole, W. & Du, Q. (2017). Microstructure evolution during homogenization of Al-Mg-Si-Mn-Fe alloys: Modelling and experimental results. *Transactions of Nonferrous Metals Society of China*. 27(4), 747-753. https://doi.org/10.1016/S1003-6326(17)60085-2.

[10] Hsu, C., O'reilly, K., Cantor, B. & Hamerton, R. (2001). Non-equilibrium reactions in 6xxx series Al alloys. *Materials Science and Engineering A*. 304-306, 119-124. https://doi.org/10.1016/S0921-5093(00)01467-2.

[11] Mrówka-Nowotnik, G., Sieniawski, J. & Nowotnik, A. (2006). Tensile properties and fracture toughness of heat treated 6082 alloy. *Journal of Achievements in Materials and Manufacturing Engineering*. 17, 1-2, 105-108.

[12] Mrówka-Nowotnik, G. & Sieniawski, J. (2005). Influence of heat treatment on the microstructure and mechanical properties of 6005 and 6082 aluminium alloys. *Journal of Materials Processing Technology*. 162-163, 367-372. https://doi.org/10.1016/j.jmatprotec.2005.02.115.

[13] Sha, G., O'Reilly, K., Cantor, B., Worth, J. & Hamerton, R. (2001). Growth related metastable phase selection in a 6xxx series wrought Al alloy. *Materials Science and Engineering A*. 304-306, 612-616. https://doi.org/10.1016/S0921-5093(00)01545-8.

[14] Carlberg, T., Bayat, N. & Erdegren, M. (2015). Surface segregation and surface defect formation during aluminum billet casting. *Transactions of the Indian Institute of Metals*. 68, 1065-1069. https://doi.org/10.1007/s12666-015-0647-0.

[15] Samaras, S. & Haidemenopoulos, G. (2007). Modelling of microsegregation and homogenization of 6061 extrudable Al-alloy. *Journal of Materials Processing Technology*.

194(1-3), 63-73. https://doi.org/10.1016/j.jmatprotec.2007.03.126.
[16] Sarafoglou, P.I., Serafeim, A., Fanikos, I.A., Aristeidakis, J. S. & Haidemenopoulos, G.N. (2019). Modeling of microsegregation and homogenization of 6xxx Al-alloys including precipitation and strengthening during homogenization cooling. *Materials*. 12(9), 1421, 1-25. https://doi.org/10.3390/ma12091421.
[17] Bao, S., Eggen, S., Syvertsen, M. & Kvithyld, A. (2023). Collection, thermal treatment, and remelting end-of-life Al packaging in Norway. *The Journal of The Minerals, Metals & Materials Society (TMS)*. 75, 5755-5763. https://doi.org/10.1007/s11837-023-06195-6.
[18] Bao, S., Kvithyld, A., Bjørlykke, G.A., Sandaunet, K. (2023). Recycling of aluminum from aluminum food tubes. In S. Broek (Eds.), *Light metals* (pp. 960-966). Springer. https://doi.org/10.1007/978-3-031-22532-1_128.
[19] Cui, J., Kvithyld, A., & Roven, H. (2010). Degreasing aluminium turnings and implications for solid state recycling. In *Light Metals* (pp. 675-678). The Minerals, Metals, and Materials Society (TMS).
[20] Dispinar, D., Kvithyld, A. & Nordmark, A. (2011). Quality assessment of recycled aluminium. In S. J. Lindsay (Eds.), *Light Metals* (pp. 731-735). Springer. https://doi.org/10.1007/978-3-319-48160-9_127.
[21] Kvithyld, A., Meskers, C., Gaal, S., Reuter, M. & Engh, T. A. (2008). Recycling light metals: Optimal thermal de-coating. *Journal of The Minerals, Metals & Materials Society*. 60, 47-51. https://doi.org/10.1007/s11837-008-0107-y.
[22] Boczkal, S., Augustyn, B., Hrabia-Wiśnios, J., Kapinos, D., Lewis, G., Bareel, P.-F., Savelli, S., da Silva, M. & Özen, T. (2023). Preparation of high-quality 6xxx aluminium eco alloys cast in billets. *Engineering Proceedings.* 43(1), 23, 1-10. https://doi.org/10.3390/engproc2023043023
[23] Rajagukguk, K., Suyitno, S., Saptoadi, H., Kusumaningtyas, I., Arifvianto, B. & Mahardika, M. (2024). Remelting of Aluminum Scrap into Billets Using Direct Chill Casting. *Archives of Foundry Engineering*. 24(1), 40-49. https://doi.org/10.24425/afe.2024.149250.
[24] Jones, S. & Rao, A.P. (2013). Melt conditioned direct chill (MC-DC) casting of Al alloys. *Transactions of the Indian Institute of Metals*. 66, 117-121. https://doi.org/10.1007/s12666-012-0235-5.
[25] Salloum-Abou-Jaoude, G., Eskin, D.G., Lebon, G.S.B., Barbatti, C., Jarry, P., Jarrett, M. (2019). Altering the microstructure morphology by ultrasound melt processing during 6XXX aluminium DC-casting. In C. Chesonis (Eds.), *Light metals* (pp. 1605-1610). Springer. https://doi.org/10.1007/978-3-030-05864-7_203.
[26] Subroto, T., Lebon, G.S., Eskin, D.G., Skalicky, I., Roberts, D., Tzanakis, I. & Pericleous, K. (2021). Numerical modelling and experimental validation of the effect of ultrasonic melt treatment in a direct-chill cast AA6008 alloy billet. *Journal of Materials Research and Technology*. 12, 1582-1596. https://doi.org/10.1016/j.jmrt.2021.03.061.
[27] Nadella, R., Eskin, D. G., Du, Q. & Katgerman, L. (2008). Macrosegregation in direct-chill casting of aluminium alloys. *Progress in Materials Science*. 53(3), 421-480. https://doi.org/10.1016/j.pmatsci.2007.10.001.
[28] Schneider, W. (2016). D.C. casting of aluminium alloys-Past, present and future. In J. F. Grandfield & D. G. Eskin (Eds.), *Essential readings in light metals* (pp. 534-541). Springer. https://doi.org/10.1007/978-3-319-48228-6_64.
[29] Campbell, J. (2003). *Castings.* (2nd ed.). Butterworth-Heinemann Ltd., Oxford, Elsevier
[30] Campbell, J. (2006). Entrainment defects. *Materials Science and Technology*. 22(2), 127-145. https://doi.org/10.1179/174328406X74248
[31] Dispinar, D., Campbell, J. (2014). Reduced pressure test (RPT) for bifilm assessment. In *Shape Casting: 5th International Symposium 2014* (pp. 243-251). Springer. https://doi.org/10.1007/978-3-319-48130-2_30.
[32] Dispinar, D. & Campbell, J. (2004). Critical assessment of reduced pressure test. Part 1: Porosity phenomena. *International Journal of Cast Metals Research*. 17(5), 280-286. https://doi.org/10.1179/136404604225020696.
[33] Dispinar, D. & Campbell, J. (2004). Critical assessment of reduced pressure test. Part 2: Quantification. *International Journal of Cast Metals Research*. 1(5), 287-294. https://doi.org/10.1179/136404604225020704
[34] Dispinar, D., Campbell, J. (2007). A comparison of methods used to assess aluminium melt quality. In Shape Casting: 2nd International Symposium, *25 February- 1 March 2007* (pp.11–18). Orlando-FL, United States: The Minerals, Metals and Materials Society (TMS)